Application of a negative stiffness mechanism on pitching wave energy devices

Kurniawan, Adi; Zhang, Xiantao

Published in:
Proceedings of the 5th Offshore Energy and Storage Symposium

Publication date:
2018

Document Version
Publisher's PDF, also known as Version of record

Proceedings of Offshore Energy and Storage 2018
Ningbo, China
July 4 - 6, 2018

Application of a Negative Stiffness Mechanism on Pitching Wave Energy Devices

Adi Kurniawan*
Department of Civil Engineering, Aalborg University
Thomas Manns Vej 23, 9220 Aalborg Ø, Denmark
Xiantao Zhang†
School of Civil, Environmental and Mining Engineering, The University of Western Australia
35 Stirling Hwy, Crawley, Perth, Western Australia 6009, Australia

Abstract

Harnessing energy from ocean waves in an economic manner remains a challenge. Recent efforts are targeted at improving the performance of a wave energy device without resorting to reactive control. One such strategy is to use a negative stiffness mechanism. Theoretically, negative stiffness is able not only to lengthen the resonance period of the device, but also to broaden its resonance bandwidth, thus making it potentially capable of capturing energy from a broader spectrum of incoming waves. This study aims to extend the application of such mechanism to pitching wave energy devices by studying Salter-duck type devices as a specific case. We consider first a single duck, and then two lines of multiple ducks meeting at an angle. The analysis is carried out using linear frequency-domain models. For this purpose, equivalent linearised stiffness of the negative stiffness mechanism is derived. Our study confirms that negative stiffness improves the power performance of pitching devices. However, it is most effective when the pitch rotation axis is fixed. It becomes less effective when the axis is allowed to move.

1. Introduction

Harnessing energy from ocean waves in an economic manner remains a challenge. Recent efforts are targeted at improving the performance of a wave energy device without resorting to reactive control. One such strategy is to use a negative stiffness mechanism, which can be applied on an oscillating body by a system of springs compressed at mean position and aligned perpendicular to the direction of motion. As long as it is in compression, the springs exert a positive force in the direction of motion and thus the body has a negative stiffness in this direction. There exists, however, other means to accomplish the same effect, such as using a system of magnets [1].

When introduced to a wave energy device, a negative stiffness mechanism is able to reduce the total stiffness of the system. This is particularly beneficial for wave energy devices, which in principle have to resonate with the waves to capture the most energy out of them [2]. With a lower stiffness, the device can have a longer resonance period for the same mass, which means that it can be made smaller in size for a given target wave period, hence reducing the cost of energy.

The benefits of a negative stiffness mechanism on heaving axisymmetric devices (point absorbers) have been highlighted by Zhang et al. [3] and Todalshaug et al. [4] through numerical and experimental studies. In addition to lengthening the resonance period, negative stiffness broadens the resonance bandwidth of the device, thus making it capable of capturing energy from a broader spectrum of incoming waves. However, the application of negative stiffness mechanism on devices other than point absorbers has so far been limited [5].

This study therefore aims to extend the application of negative stiffness on pitching wave energy devices. Devices resembling the Salter duck [6] are chosen as a specific case. We first study the application of negative stiffness to a single duck, and then to two lines of multiple ducks meeting at an angle. While a number of studies exist on a single duck [7–14], much fewer studies on arrays of ducks have been reported [15, 16]. This study therefore also serves to fill this gap.

Our analysis is carried out using linear frequency-domain models. For this purpose, equivalent linearised stiffness of the spring system will be derived in section 2. The frequency-domain models of the single duck and the multiple ducks are described in sections 3 and 4. In section 5, the anticipated benefits of the negative stiffness mechanism are evaluated via comparison with the same models but without the negative stiffness. Section 6 concludes the paper.

* Assistant professor, corresponding author, aku@civil.aau.dk
† PhD candidate

2. Linearised stiffness of negative spring systems

2.1. Heaving body

The negative spring mechanism is described by Ramlan et al. [17] and is most easily understood by considering the system illustrated in Fig. 1. At mean position, one end of the spring is fixed at point A and the other end is attached to point B. The spring is compressed at this position and is aligned perpendicular to the direction of motion, the vertical direction. As long as it is in compression, the spring therefore exerts a force with a positive component in the direction of motion and thus has a negative restoring stiffness in this direction. This is in contrast to a spring aligned parallel to the direction of motion, in which case it exerts a force opposing the motion and thus has a positive restoring stiffness.

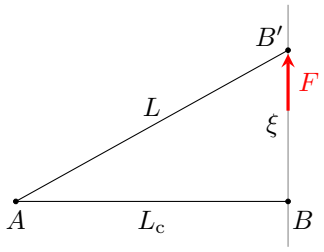

Figure 1. Negative spring mechanism on a heaving body.

The force F exerted by the spring in the direction of motion can be derived by observing Fig. 1. At its mean position, the length of the compressed spring is minimum and is equal to L_c. As the body heaves by ξ, point B moves to B' and the spring's length increases to L. From the figure,

$$L = \sqrt{L_c^2 + \xi^2}. \tag{1}$$

The force exerted by the spring is linear along its axis, but nonlinear in the vertical direction. If we denote the unloaded length of the spring by L_0 (where $L_0 \geq L_c$) and the spring rate by K, the vertical force exerted by the spring on the heaving body is then

$$F = K(L_0 - L)\frac{\xi}{L}. \tag{2}$$

Substituting (1) into (2), we have

$$F = K\left(\frac{L_0}{\sqrt{L_c^2 + \xi^2}} - 1\right)\xi, \tag{3}$$

which is nonlinear in ξ. For small ξ, a linear approximation to (3) is

$$F \approx K\left(\frac{L_0}{L_c} - 1\right)\xi, \tag{4}$$

such that the linearised negative stiffness of the spring mechanism is equal to $K\,(1 - L_0/L_c)$ for a heaving body.

As an example, the variations of vertical force and length of spring for $L_c/L_0 = 2/3$ are plotted in Fig. 2. When $L = L_0$, for which $\xi/L_0 = \sqrt{1 - L_c^2/L_0^2}$, the force exerted by the spring is zero. For $L > L_0$, the spring is in tension and therefore the force reverses in direction. The linearised force, given by (4), is shown in the figure as the dashed line. Obviously, the linear approximation becomes less accurate as the displacement ξ gets larger.

The hydrostatic stiffness K_s of a heaving body is given by Archimedes principle and is equal to $\rho g S_w$, where ρ is the water density, g is the acceleration due to gravity, and S_w is the water plane area of the body. It is implicitly assumed that the body is cylindrical, i.e. it has a uniform horizontal cross section.

The total restoring force F_s is given as $K_s\xi - F$. This F_s, normalised by $K_s\xi$, for $K_s = 3K$, is plotted in Fig. 3a as the solid line. The negative spring is seen to reduce the total restoring force such that it is less than the hydrostatic restoring force in the region where $L < L_0$. When $L > L_0$, the spring is in tension and the total stiffness is greater than the hydrostatic stiffness. The linearised total restoring force is shown as the horizontal dashed line. The corresponding ratio of the linearised to the exact hydrostatic force is shown in Fig. 3b. Whether the linearised version is a good approximation of the exact force depends on the magnitude of F relative to $K_s\xi$, which in turn depends on the K_s/K and L_c/L_0 ratios. The approximation gets better with higher K_s/K and L_c/L_0 ratios.

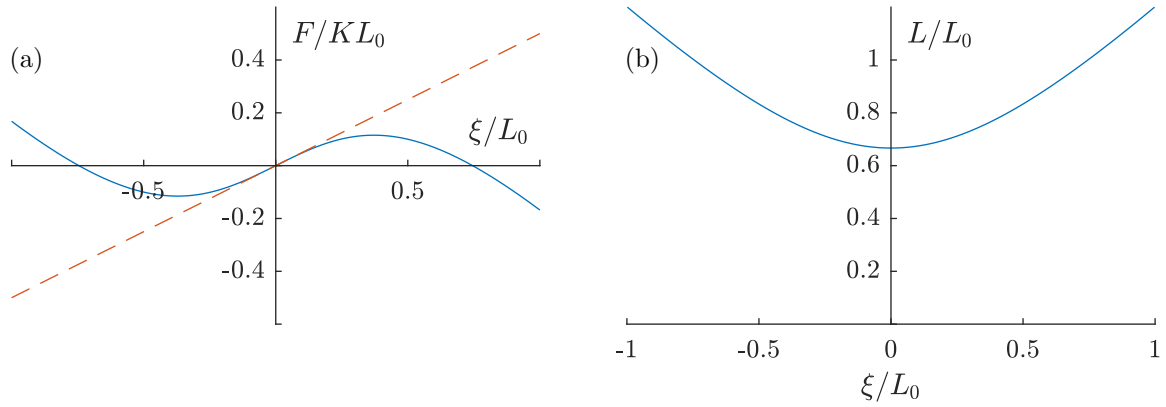

Figure 2. (a) Vertical force and (b) length of spring as functions of heave displacement.

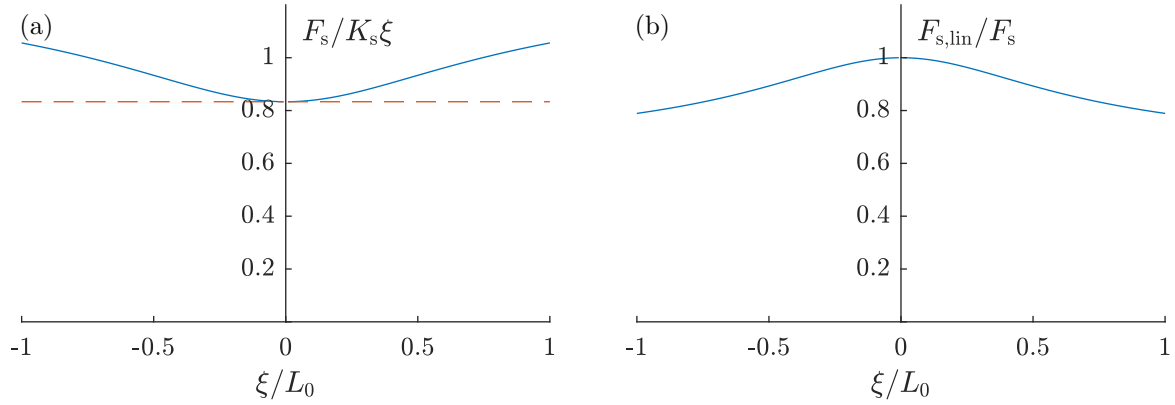

Figure 3. (a) Heave restoring force and (b) ratio of the linearised restoring force to the exact restoring force, as functions of heave displacement.

2.2. *Pitching body*

A simple arrangement of the negative spring mechanism on a pitching body is illustrated in Fig. 4. One end of the spring is fixed at point A and the other end is attached to point B. At its mean position, the length of the compressed spring is minimum and is equal to L_c. As the body pitches by ξ about O, point B moves to B' and the spring's length increases to L. From the figure,

$$\begin{aligned} L &= \sqrt{[L_c + R(1-\cos\xi)]^2 + R^2\sin^2\xi} \\ &= \sqrt{L_c^2 + 2R(L_c+R)(1-\cos\xi)}. \end{aligned} \tag{5}$$

If we denote the unloaded length of the spring by L_0 and the spring rate by K, the moment exerted by the spring about point O is then

$$M = FR\cos\beta = K(L_0 - L)R\cos\beta. \tag{6}$$

Noting that

$$R\cos\beta = (L_c + R)\sin\gamma \tag{7}$$

and

$$L\sin\gamma = R\sin\xi, \tag{8}$$

we can rewrite (6) as

$$M = K(L_0 - L)\frac{L_c + R}{L}R\sin\xi. \tag{9}$$

For small ξ, $\cos\xi \approx 1$ and $\sin\xi \approx \xi$, and a linear approximation of (9) is obtained as

$$M \approx K\left(\frac{L_0}{L_c} - 1\right)(L_c + R)R\xi, \tag{10}$$

such that the linearised negative stiffness of the mechanism is equal to $K\,(1 - L_0/L_c)\,(L_c + R)R$ for a pitching body.

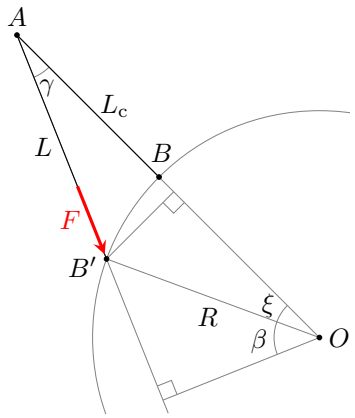

Figure 4. Snap-through mechanism on a pitching body.

As an example, the variations of moment and length of spring for $L_c/L_0 = 2/3$ are plotted in Fig. 5. When $L = L_0$, the force exerted by the spring is zero. For $L > L_0$, the spring is in tension and therefore the force reverses in direction. The linearised moment, given by (10), is shown in the figure as the straight line.

Whereas in the heaving body the spring's length L can increase indefinitely with ξ so long as it does not break, in the pitching body the spring's length L cannot theoretically be greater than $L_{\max} = L_c + 2R$. Also, since we know that the spring's moment arm is zero at $\xi = \pm\pi$, the moment due to the spring is bounded.

The hydrostatic restoring moment on a pitching body is a nonlinear function of the pitch displacement ξ, but for simplicity, we assume it to be linearly proportional to ξ. The total restoring moment M_s, for $K_s = 3.125KL_0R$, is shown as the solid line in Fig. 6a. The linearised total restoring moment is shown as the horizontal dashed line. The corresponding ratio of the linearised moment to the 'exact' moment is shown in Fig. 6b.

3. Frequency-domain model of a single duck

Consider a single duck pitching about a horizontal axis passing through point O, as shown in Fig. 7. Each half of the vertical cross-sectional profile is defined by two circular arcs of different radii, R_a and R_f. This cross section differs slightly from the original duck cross section proposed by Salter [6], which is made up of two arcs of different radii and a straight line. The width of the duck is denoted by d. A right-handed Cartesian coordinate system is used with the Z-axis pointing upward and the plane $Z = 0$ defining the mean free surface. The angle of propagation β of the incident waves is measured relative to the X-axis. The incident waves propagate along the X-axis when $\beta = 0$.

At rest, the sum of forces acting on the body (the buoyancy force, the gravitational force, and the reaction force on the axis) is zero, and the buoyancy moment about the axis of rotation is equal and opposite to the gravitational moment about the same axis.

3.1. Fixed axis of rotation

For a duck pitching about a fixed axis of rotation, the equation of motion describing the angular displacement ξ_7 about the fixed axis can be written as

$$[\mathrm{i}\omega(I + A_{77}) + B_{77} + B_{\mathrm{PTO}} + (C_{77} + C_{\mathrm{PTO}})/\mathrm{i}\omega]\, U_7 = F_{\mathrm{e},7}, \tag{11}$$

where I is the moment of inertia of the body about the axis of rotation, A_{77} and B_{77} are the corresponding added inertia and radiation damping, B_{PTO} and C_{PTO} are the applied power take-off (PTO) damping and stiffness, C_{77} is the restoring stiffness, $U_7 = \mathrm{i}\omega\xi_7$ is the angular velocity of the body about the axis of rotation, and $F_{\mathrm{e},7}$ is the excitation moment due to the incident waves.

Denoting the mass of the body by M, the submerged volume by $\forall$, the centre of buoyancy by B, and the centre of gravity by G, we may express the restoring stiffness C_{77} as

$$C_{77} = \rho g \int_{S_w} (X - X_O)^2 \mathrm{d}S + \rho g \forall (Z_B - Z_O) + Mg(Z_O - Z_G). \tag{12}$$

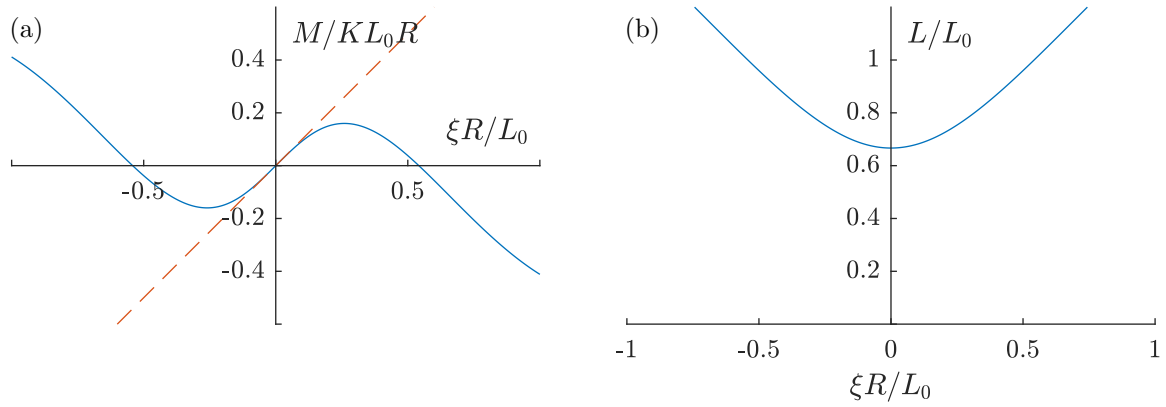

Figure 5. (a) Moment and (b) length of spring as functions of pitch angular displacement.

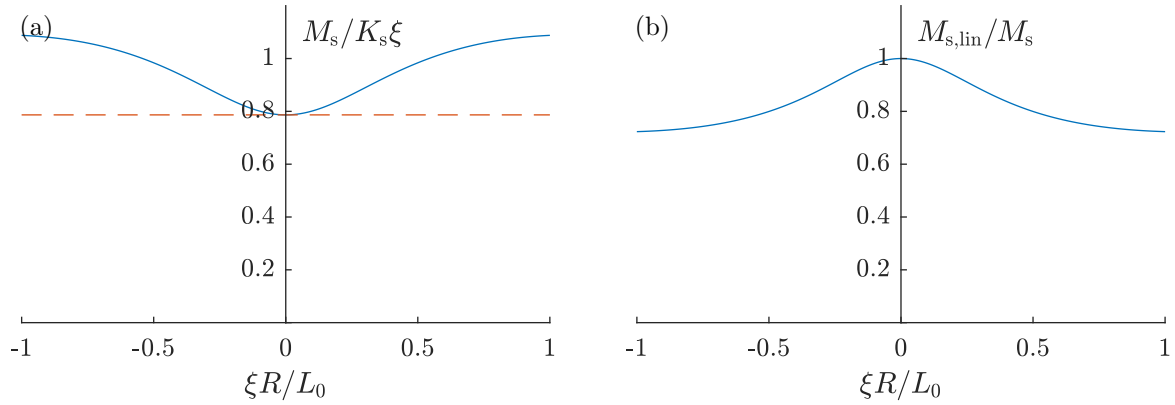

Figure 6. (a) Pitch restoring moment and (b) ratio of the linearised restoring moment to the 'exact' restoring moment, as functions of pitch angular displacement.

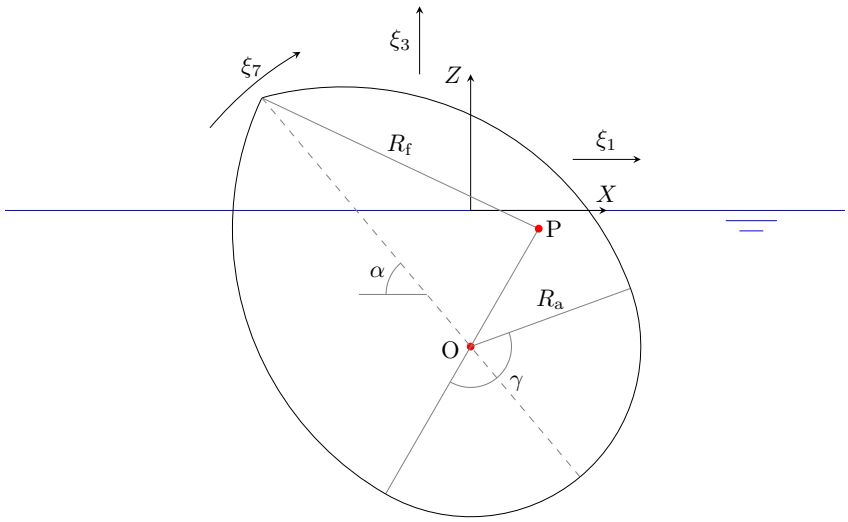

Figure 7. Notations for a single duck (side view).

Here, the first term is the second area moment of the water plane area S_w about the axis of rotation projected on the mean free surface. The first and second terms are the contribution due to hydrostatic pressures, while the third is due to gravity.

The mean power P absorbed through the pitch motion is

$$P = \frac{1}{2} B_{PTO} |U_7|^2. \tag{13}$$

3.2. Compliant axis of rotation

When the axis of rotation is allowed to move in surge ($j=1$) and heave ($j=3$), the displacement of any point $\mathbf{X}$ on the body due to a motion in mode j is given as the product of the displacement amplitude ξ_j and the shape function $\mathbf{S}_j$, with

$$\mathbf{S}_j = \begin{cases} \mathbf{i} & \text{for } j=1 \\ \mathbf{k} & \text{for } j=3\,, \\ (Z-Z_\mathrm{O})\mathbf{i}-(X-X_\mathrm{O})\mathbf{k} & \text{for } j=7 \end{cases} \tag{14}$$

where $\mathbf{i},\mathbf{j},\mathbf{k}$ are the unit vectors in X-, Y-, and Z-directions. The equation of motion for the body can be written in matrix form as

$$[\mathrm{i}\omega(\mathbf{M}+\mathbf{A})+\mathbf{B}+\mathbf{B}_\mathrm{PTO}+(\mathbf{C}+\mathbf{C}_\mathrm{PTO})/\mathrm{i}\omega]\,\mathbf{U} \equiv (\mathbf{Z}_\mathrm{PTO}+\mathbf{Z})\,\mathbf{U} = \mathbf{F}_\mathrm{e}, \tag{15}$$

where $\mathbf{Z}$ is defined as the intrinsic impedance.

The elements of the mass matrix $\mathbf{M}$ are evaluated from

$$M_{ij} = \int_V \rho_\mathrm{M}\mathbf{S}_i\cdot\mathbf{S}_j\mathrm{d}V, \tag{16}$$

where ρ_M is the mass density of the body and V is the volume of the body. The non-zero elements are obtained as

$$M_{11} = M_{33} = M \tag{17}$$
$$M_{17} = M_{71} = M(Z_\mathrm{G}-Z_\mathrm{O}) \tag{18}$$
$$M_{37} = M_{73} = -M(X_\mathrm{G}-X_\mathrm{O}) \tag{19}$$
$$M_{77} = I. \tag{20}$$

The hydrostatic part of the restoring stiffness can be evaluated from [18]

$$K_{ij} = \rho g\int_{S_\mathrm{B}} n_j(w_i+ZD_i)\mathrm{d}S, \tag{21}$$

where $n_j=\mathbf{S}_j\cdot\mathbf{n}$ is the normal component of $\mathbf{S}_j$, w_i is the z-component of $\mathbf{S}_i$, and $D_i=\nabla\cdot\mathbf{S}_i$ is the divergence of $\mathbf{S}_i$. The non-zero elements are obtained as

$$K_{33} = \rho g S_\mathrm{w} \tag{22}$$
$$K_{37} = K_{73} = -\rho g\int_{S_\mathrm{w}}(X-X_\mathrm{O})\mathrm{d}S \tag{23}$$
$$K_{71} = \rho g\forall \tag{24}$$
$$K_{77} = \rho g\int_{S_\mathrm{w}}(X-X_\mathrm{O})^2\mathrm{d}S+\rho g\forall(Z_\mathrm{B}-Z_\mathrm{O}). \tag{25}$$

The total restoring stiffness includes the contributions due to gravity and the reaction force on the axis of rotation. Thus, $C_{ij}=K_{ij}$ except

$$C_{71} = 0 \tag{26}$$
$$C_{77} = K_{77}+Mg(Z_\mathrm{O}-Z_\mathrm{G}). \tag{27}$$

The mean absorbed power is

$$P = \frac{1}{2}\mathbf{U}^\dagger\mathbf{B}_\mathrm{PTO}\mathbf{U}, \tag{28}$$

where † denotes the complex conjugate transpose. The PTO damping matrix $\mathbf{B}_\mathrm{PTO}$ is herein assumed to be diagonal, that is, the PTO force applied in each mode depends on the motion of that mode only. Then, (28) equals to

$$P = \frac{1}{2}\sum_j B_{\mathrm{PTO},jj}|U_j|^2. \tag{29}$$

The reaction forces and moment on the rotation axis can be obtained from

$$\mathbf{F}_\mathrm{react} = \mathbf{Z}\mathbf{U}-\mathbf{F}_\mathrm{e}. \tag{30}$$

Equation (15) can be regarded as a more general version of (11). If any of the modes $j\in\{1,3,7\}$ is fixed, we know that $U_j=0$ and only the velocities for the remaining modes are solved using (15). Thus (15) reduces to (11) when modes $j=1,3$ are fixed. In any case, however, the reaction force vector $\mathbf{F}_\mathrm{react}$ must be calculated using the full $\mathbf{Z}$ and $\mathbf{F}_\mathrm{e}$.

4. Frequency-domain model of two lines of ducks meeting at an angle

Next, we shall consider wave energy absorption by two lines of ducks meeting at an angle, as shown in Fig. 8. The system represents a platform with two arms, where N ducks are mounted on each arm and thus having a common rotation axis. The configuration is similar to the WEPTOS [19], a wave energy device under development in Denmark.

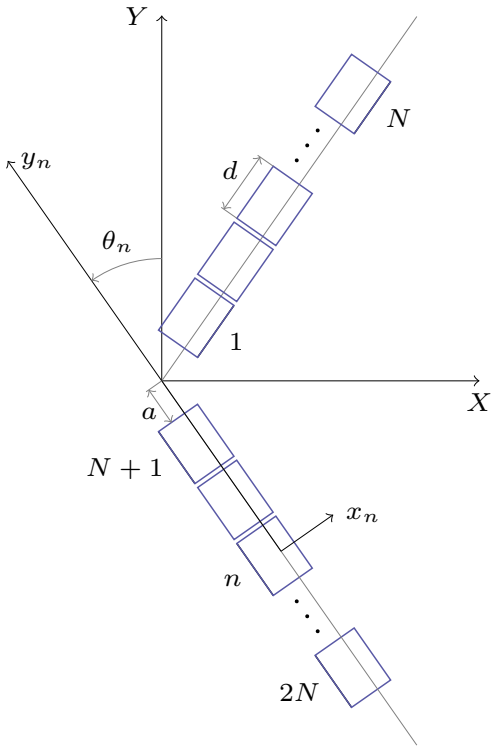

Figure 8. Notations for two lines of ducks meeting at an angle (plan view).

A right-handed Cartesian coordinate system is defined such that the system at rest is symmetrical about $Y = 0$ and the fluid domain occupies $Z \leq 0$. The coordinate system of duck n is defined such that the y_n-axis coincides with the axis of rotation, the duck is symmetrical about $y_n = 0$, and the z_n-axis points upwards.

The system has in general $6+2N$ degrees of freedom, six being the rigid body modes of the whole system and $2N$ being the independent rotations of each duck about its axis. However, we assume that the system is always symmetrical with respect to the incident wave direction, i.e. the incident wave propagates along the X-axis. In addition, we assume that ducks n and $N+n$, $n = 1,\ldots,N$ have the same PTO impedance. Because of this symmetry, the degrees of freedom reduce to $3+N$. We reserve the index $j = 1,\ldots,6$ for the conventional rigid body modes of the whole system. Thus, $j = 1,3,5$ denote the surge, heave, and pitch of the whole system as a single body. In addition, $j = 7,\ldots,N+6$ denote the additional N modes describing the motion of the ducks relative to the platform.

The displacement of any point $\mathbf{X}$ on the system due to a motion in mode j is given as the product $\xi_j \mathbf{S}_j$. The shape functions $\mathbf{S}_j$ for $j = 1,3,5$ are given as

$$\mathbf{S}_j = \begin{cases} \mathbf{i} & \text{for } j = 1 \\ \mathbf{k} & \text{for } j = 3 \\ Z\mathbf{i} - X\mathbf{k} & \text{for } j = 5 \end{cases} \tag{31}$$

for all $\mathbf{X}$ in the body.

The displacement of a point $\mathbf{x}_n$ on duck n due to a unit rotation about its axis is given in its own coordinate system as

$$\mathbf{S}_{\mathrm{p}n} = z_n \mathbf{i}_n - x_n \mathbf{k}_n. \tag{32}$$

Denoting $\mathbf{X}_{\mathrm{O}n}$ as the origin of the duck coordinate system (measured in the global coordinate system) and θ_n as the angle of the y_n-axis relative to the Y-axis, we have the following relations between the duck's and the global

coordinates and unit vectors:

$$x_n = (X - X_{On})\cos\theta_n + (Y - Y_{On})\sin\theta_n \tag{33}$$
$$z_n = Z - Z_{On} \tag{34}$$
$$\mathbf{i}_n = \mathbf{i}\cos\theta_n + \mathbf{j}\sin\theta_n \tag{35}$$
$$\mathbf{k}_n = \mathbf{k}, \tag{36}$$

which, upon substitution into (32), yield

$$\mathbf{S}_{pn} = (Z - Z_{On})\cos\theta_n\,\mathbf{i} + (Z - Z_{On})\sin\theta_n\,\mathbf{j} - [(X - X_{On})\cos\theta_n + (Y - Y_{On})\sin\theta_n]\mathbf{k} \tag{37}$$

in terms of the global coordinates and unit vectors. Due to symmetry, $\theta_{N+n} = -\theta_n$.

The modes $j = 6+n$ for $n = 1,\ldots,N$ are defined as positive rotations of equal magnitude of duck n and $N+n$ about their respective axes. In terms of shape functions,

$$\mathbf{S}_{j|j=6+n,n=1,\ldots,N} = \begin{cases} \mathbf{S}_{pn} & \text{for } \mathbf{X} \in D_n \\ \mathbf{S}_{pN+n} & \text{for } \mathbf{X} \in D_{N+n} \\ 0 & \text{elsewhere} \end{cases}, \tag{38}$$

where D_n is the region occupied by duck n.

The equation of motion for the system can be written in matrix form as (15) and once the angular velocities of the ducks are solved for, the mean absorbed power can be obtained from (28), bearing in mind that since there are in total $2N$ ducks, the values of $B_{\mathrm{PTO},jj}$ and $C_{\mathrm{PTO},jj}$ for $j = 7,\ldots,N+6$ have to be twice the values applied on each duck.

Having defined the shape functions $\mathbf{S}_j$, we can evaluate the elements of the mass matrix $\mathbf{M}$ from (16). The non-zero elements are

$$M_{11} = M_{33} = M \tag{39}$$
$$M_{15} = M_{51} = MZ_{\mathrm{G}} \tag{40}$$
$$M_{35} = M_{53} = -MX_{\mathrm{G}} \tag{41}$$
$$M_{55} = I \tag{42}$$
$$M_{1j} = M_{j1} = 2M_{\mathrm{D}}z_{n\mathrm{G}}\cos\theta_n \tag{43}$$
$$M_{3j} = M_{j3} = -2M_{\mathrm{D}}x_{n\mathrm{G}} \tag{44}$$
$$M_{5j} = M_{j5} = 2\int_{D_n} \rho_{\mathrm{M}}(Zz_n\cos\theta_n + Xx_n)\mathrm{d}V \equiv 2I_{YD_n} \tag{45}$$
$$M_{jj} = 2I_{\mathrm{D}} \tag{46}$$

for $j = 6+n, n = 1,\ldots,N$, and where M is the total mass of the system, I is the moment of inertia of the system about the Y-axis, M_{D} is the mass of a single duck, I_{D} is the moment of inertia of a single duck about its axis of rotation, and I_{YD_n} is as defined. Also, $\mathbf{X}_{\mathrm{G}}$ is the centre of gravity of the whole system and $\mathbf{x}_{n\mathrm{G}}$ is the centre of gravity of duck n in its coordinate system.

The hydrostatic part of the restoring stiffness can be evaluated from (21). The non-zero elements are

$$K_{33} = \rho g S_{\mathrm{w}} \tag{47}$$
$$K_{35} = K_{53} = -\rho g\int_{S_{\mathrm{w}}} X\mathrm{d}S \tag{48}$$
$$K_{51} = \rho g\forall \tag{49}$$
$$K_{55} = \rho g\int_{S_{\mathrm{w}}} X^2\mathrm{d}S + \rho g\forall Z_{\mathrm{B}} \tag{50}$$
$$K_{3j} = K_{j3} = -2\rho g\int_{S_{wn}} x_n\mathrm{d}S \tag{51}$$
$$K_{j1} = 2\rho g\forall_n\cos\theta_n \tag{52}$$
$$K_{5j} = 2\rho g\int_{S_{wn}} Xx_n\mathrm{d}S + 2\rho g\forall_n z_{n\mathrm{B}}\cos\theta_n \tag{53}$$
$$K_{j5} = 2\rho g\int_{S_{wn}} Xx_n\mathrm{d}S + 2\rho g\forall_n Z_{\mathrm{B}n}\cos\theta_n \tag{54}$$
$$K_{jj} = 2\rho g\int_{S_{wn}} x_n^2\mathrm{d}S + 2\rho g\forall_n z_{n\mathrm{B}}, \tag{55}$$

Table 1. Parameters of the single duck.

Parameter [unit]	Value
M [kg]	9.309×10^4
I [kg m^2]	8.259×10^5
X_{G} [m]	-1.441
Z_{G} [m]	-4.028
R_{a} [m]	2.94
R_{f} [m]	5.88
width d [m]	7.056
X_{O} [m]	0
Z_{O} [m]	-3.146
X_{B} [m]	-0.539
Z_{B} [m]	-2.756
α [deg]	50.5
γ [deg]	150
$\forall$ [m^3]	242.72
water depth h [m]	20

for $j = 6+n, n = 1,\ldots,N$, and where S_{w} and $\forall$ are the total water plane area and displaced volume of the whole system, Z_{B} is the Z-coordinate of the centre of buoyancy of the whole system, $S_{\mathrm{w}n}$ and $\forall_n$ are the water plane area and displaced volume of duck n, while $z_{n\mathrm{B}}$ and $Z_{\mathrm{B}n}$ are the z_n- and Z-coordinates of the duck's centre of buoyancy.

The total restoring stiffness includes the contributions due to gravity and any reaction force on the axis of rotation. It also must take into account any displacement of the duck's centre of rotation due to the rigid body modes of the whole system. Thus, $\mathbf{C} = \mathbf{K}$ except for

$$C_{51} = C_{j1} = 0 \tag{56}$$
$$C_{55} = K_{55} - MgZ_{\mathrm{G}} \tag{57}$$
$$C_{5j} = C_{j5} = K_{5j} - 2M_{\mathrm{D}}gz_{n\mathrm{G}}\cos\theta_n \tag{58}$$
$$C_{jj} = K_{jj} - 2M_{\mathrm{D}}gz_{n\mathrm{G}}, \tag{59}$$

where $j = 6+n, n = 1,\ldots,N$.

For simplicity, we assume that the platform is transparent to the waves and we neglect the gaps between neighbouring ducks on each arm. Thus, defining

$$Y_{\mathrm{l}n} \equiv X\tan\theta_n + [a + d(n-1)]/\cos\theta_n \tag{60}$$
$$Y_{\mathrm{r}n} \equiv X\tan\theta_n + (a + dn)/\cos\theta_n, \tag{61}$$

where a is defined in Fig. 8, we have

$$Y_{\mathrm{l}n} \le |Y| \le Y_{\mathrm{r}n} \quad \text{for } \mathbf{X} \in D_n \bigcup D_{N+n}, n = 1,\ldots,N. \tag{62}$$

Furthermore, the XY-coordinates of the origin of duck n, for $n = 1,\ldots,N$, are given as

$$X_{\mathrm{O}n} = -[a + d(n-1/2)]\sin\theta_n \tag{63}$$
$$Y_{\mathrm{O}n} = [a + d(n-1/2)]\cos\theta_n. \tag{64}$$

5. Results and discussion

5.1. A single duck

We consider a single duck with parameters given in Table 1. The submerged geometry is shown in Fig. 9. At rest, there is an upward force of 1.53 MN on the axis of rotation due to net buoyancy. The incident waves propagate along the X-axis ($\beta = 0$). The added mass, radiation damping, and wave excitation force coefficients for the given geometry are calculated numerically using a panel method [20].

The effects of applying different negative stiffnesses on the single duck are shown in Fig. 10. Here, the PTO damping is kept constant and is equal to 10^6 Nms. Applying the negative stiffness is seen to improve the power

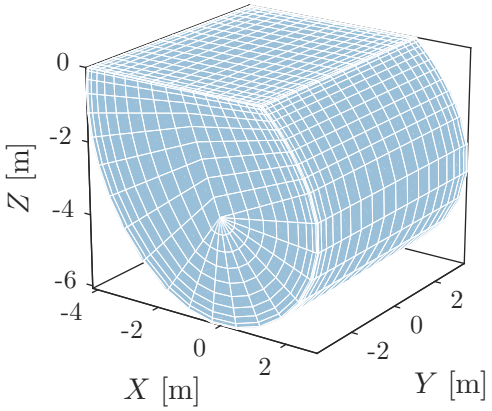

Figure 9. Panel model of a single duck with dimensions specified in table 1. The interior free surface is panelled for the purpose of removing irregular frequency effects.

capture. The peak period is lengthened, and the power curve is broadened. The undamped and uncoupled pitch resonance periods of the duck for the different negative stiffnesses can be obtained by finding the period at which the total reactance of the system is zero in each case. From this analysis, we find that the resonance period is lengthened from 3.40 s without negative stiffness to 4.84 s, 6.06 s, 7.16 s, and 8.61 s with negative stiffness. This improved power performance however comes at the price of larger pitch displacement and reaction moment on the support structure. Nevertheless, the surge reaction force stays about the same, while the increase in the heave reaction force is not as significant as that in pitch.

The linearised negative stiffness in pitch due to a negative spring with a spring rate K, original length L_0, and compressed length L_c has been derived earlier. Thus,

$$C_{\mathrm{PTO}} = K\,(1 - L_0/L_{\mathrm{c}})\,(L_{\mathrm{c}} + R)R, \tag{65}$$

where R is the distance between the duck's rotation axis and the point of application of the spring force (see Fig. 4). Assuming $R = L_c = 4$ m, we can obtain the required spring rate K as a function of the original length L_0, for different negative stiffness C_{PTO} values (see Fig. 11). For $L_0/L_c = 1.5$, the required spring rate is $K = 8.125 \times 10^4$ N/m to obtain a negative stiffness value of $C_{\mathrm{PTO}} = -1.3 \times 10^6$ Nm, and $K = 1.75 \times 10^5$ N/m to obtain $C_{\mathrm{PTO}} = -2.8 \times 10^6$ Nm.

The predictions shown in Fig. 10 must be treated as optimistic predictions. As seen from Fig. 12, the linearised restoring moment due to the negative spring arrangement becomes less accurate with increasing pitch displacement, and the range of validity of the linearised theory becomes narrower with increasing negative stiffness.

5.2. Two lines of ducks meeting at an angle

For the two lines of ducks, each duck has the same mean geometry as that of the single duck described in the previous section. However, the entire system is now assumed to be freely floating, so there is no force on the axes of rotation when the system is at rest. This means that we must increase the mass of each duck to balance its buoyancy and shift its centre of gravity so that $x_{n\mathrm{G}} = x_{n\mathrm{B}}$. The vertical coordinate of the centre of gravity $z_{n\mathrm{G}}$ is assumed to be higher than that in the previous case. With this modification of the mass properties, the undamped and uncoupled pitch resonance periods of each duck are now 4.56 s without negative spring, and 5.67 s, 6.88 s, 7.90 s, and 9.08 s with the same values of negative stiffness as in the previous case. The total moment of inertia I and horizontal coordinate of the centre of gravity X_{G} of the entire system depend on the angle between the two lines.

As a case study we analyse two lines of ten ducks $(N = 10)$ meeting at 120 degrees. The panel model is shown in Fig. 13. The incident waves propagate along the X-axis. To each duck, we apply the same set of negative stiffnesses as in the single duck case. The entire system is freely floating.

The response of the device is shown in Fig. 14, where results pertaining to individual ducks, i.e. the reaction moment $F_{\mathrm{react},n}$ and the duck displacement ξ_n, are averaged over all ducks. We find that applying negative stiffness in this case actually degrades the power performance of the device and increases the reaction moment on each duck. The only advantage, it seems, is that the displacements of the platform are reduced. It is worth noting that for this configuration the pitch natural period of the whole system is 7.12 s while the heave natural period is 6.60 s.

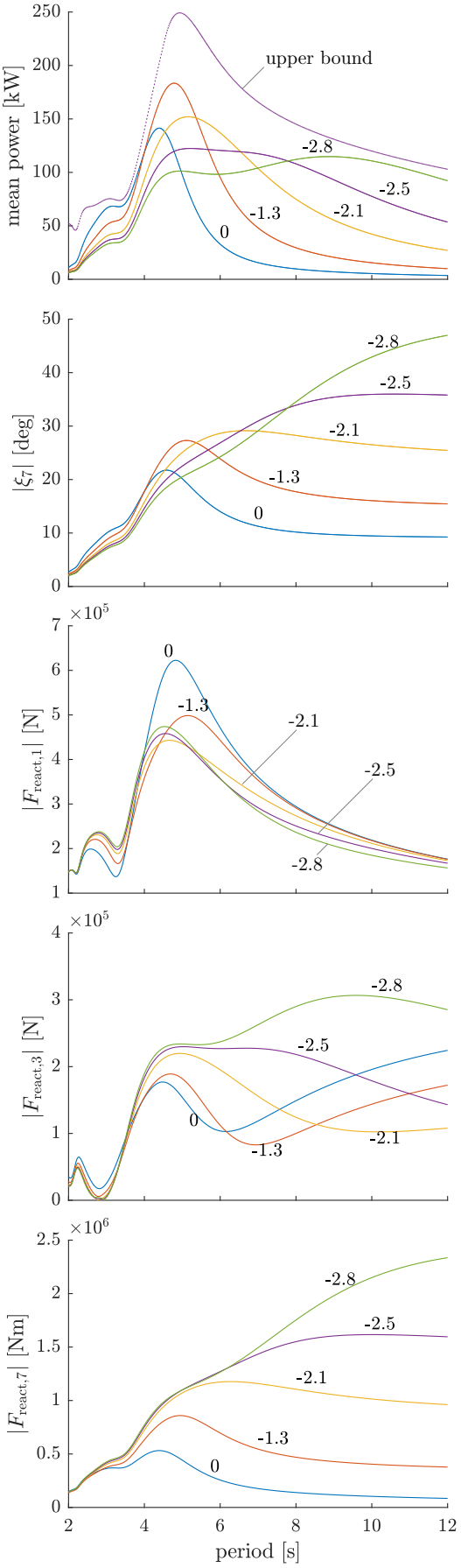

Figure 10. Mean absorbed power, pitch displacement amplitude, and reaction force (moment) amplitudes in surge, heave and pitch, for a single duck with parameters given in Table 1, a constant PTO damping of 10^6 Nms, and different negative stiffnesses as indicated (in 10^6 Nm), and for incident wave amplitude of 1 m. On the mean power plot, the upper bound when the pitch displacement is not allowed to exceed 45° for all wave periods is also shown.

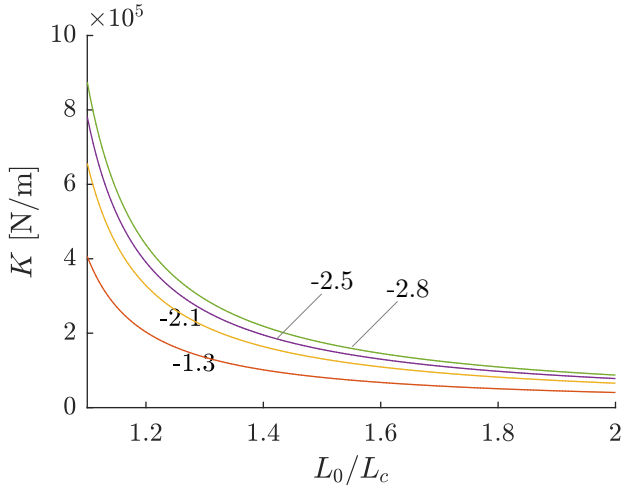

Figure 11. Required spring rate as a function of original-to-compressed spring length ratio, for $R = L_c = 4$ m and different negative stiffness values (in 10^6 Nm) as indicated.

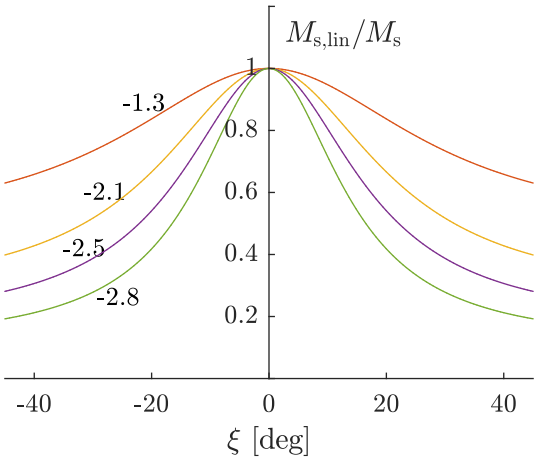

Figure 12. Ratio of linearised restoring moment to 'exact' restoring moment, as function of pitch displacement, for $R = L_c = 4$ m, $L_0/L_c = 1.5$, and different negative stiffness values (in 10^6 Nm) as indicated.

Table 2. Parameters of the two lines of ducks. Each duck has the same geometry as that of the single duck discussed in section 5.1, so the rest of the parameters in Table 1 applies to each duck.

Parameter [unit]	Value
a [m]	5.292
M_{D} [kg]	2.488×10^5
I_{D} [kg m^2]	1.529×10^6
$x_{n\mathrm{G}}$ [m]	-0.539
$Z_{n\mathrm{G}}$ [m]	-3.587

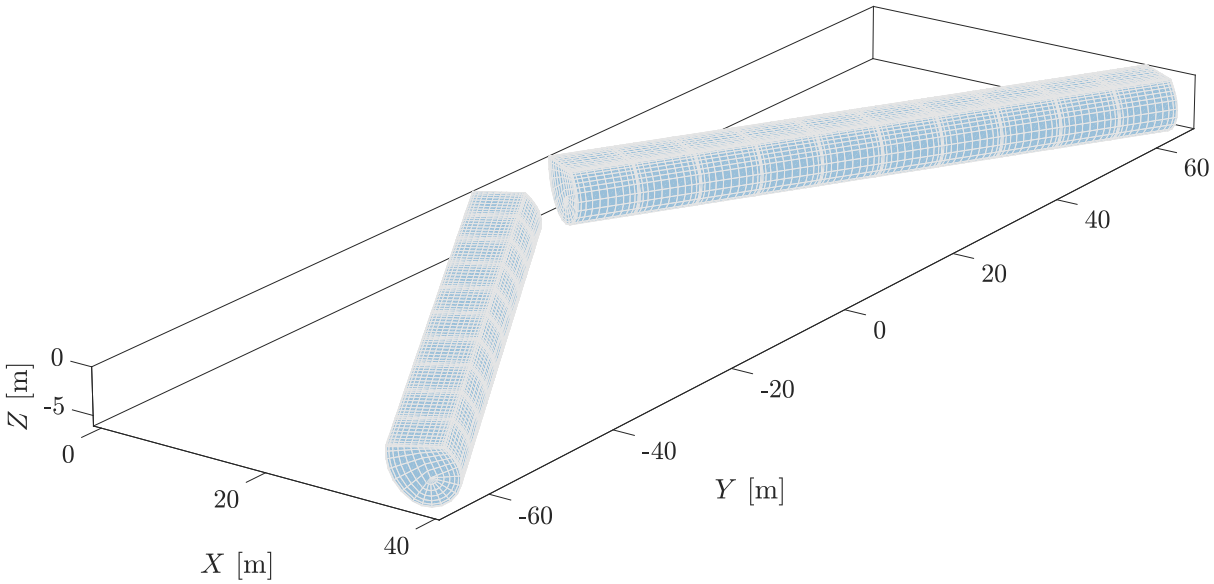

Figure 13. Panel model of two lines of ten ducks meeting at 120 degrees.

The amplified displacements of the platform around these periods appear to be responsible for the sharp decline of the absorbed power at around 7 s. For wave periods greater than 7 s, the motion of the platform follows the waves and therefore a stable reference for the ducks to react against is lost.

We confirm that this is indeed the case by analysing the same system, but with the platform fixed. In this case a stable reference exists and the negative spring works effectively in improving the power performance (Fig. 15). The change in the device response with increasing negative stiffness is similar to that for the single duck (see Fig. 10), whose rotation axis is also fixed.

6. Conclusion

The effects of a negative stiffness mechanism on pitching wave energy devices have been investigated through a numerical study. Our study confirms that negative stiffness lengthens the resonance period and broadens the resonance bandwidth of pitching devices, at the price of larger displacements and reaction forces. The mechanism is most effective when the pitch rotation axis is fixed. It becomes less effective when the axis is allowed to move.

As is often the case with results obtained from linear analyses, the results presented herein must be treated as optimistic estimates. A natural extension of this study would be to include the exact nonlinear expression of the negative stiffness in a time-domain model, which may also include the nonlinear dependence of the hydrostatic restoring moment on the pitch displacement, and losses, which so far have been neglected. These may give a more conservative estimate of the effects of the negative stiffness mechanism on these devices, although we believe that they would not change our main conclusion.

Acknowledgements

Supports from OES-BECS, INORE, and Det Obelske Familiefond are gratefully acknowledged.

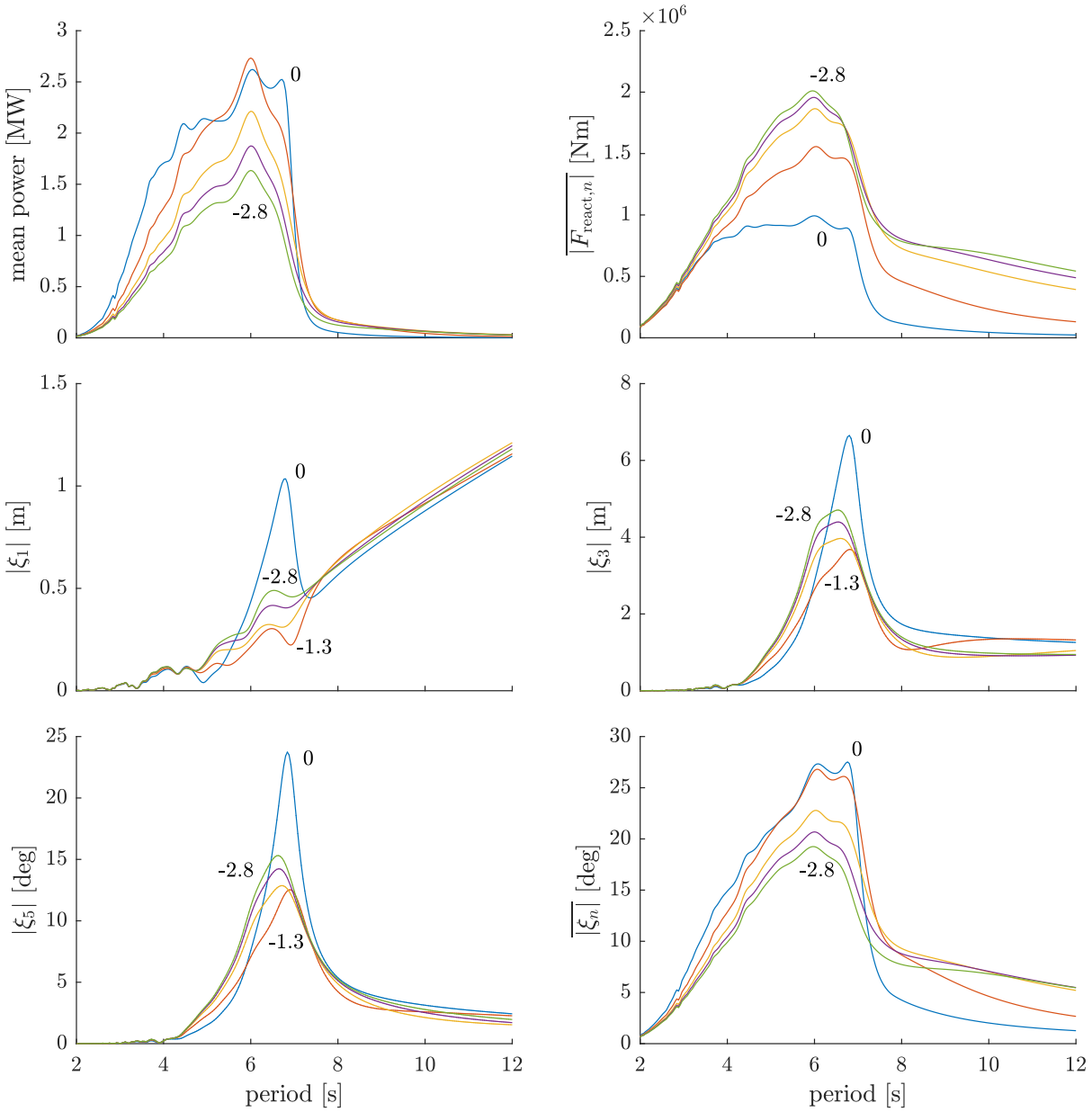

Figure 14. Mean absorbed power, reaction moment amplitudes, and displacement amplitudes for a system consisting of two lines of ten ducks ($N = 10$) meeting at 120 degrees, with parameters given in Table 2, a constant PTO damping of 10^6 Nms, and different negative stiffnesses (in 10^6 Nm), and for incident wave amplitude of 1 m.

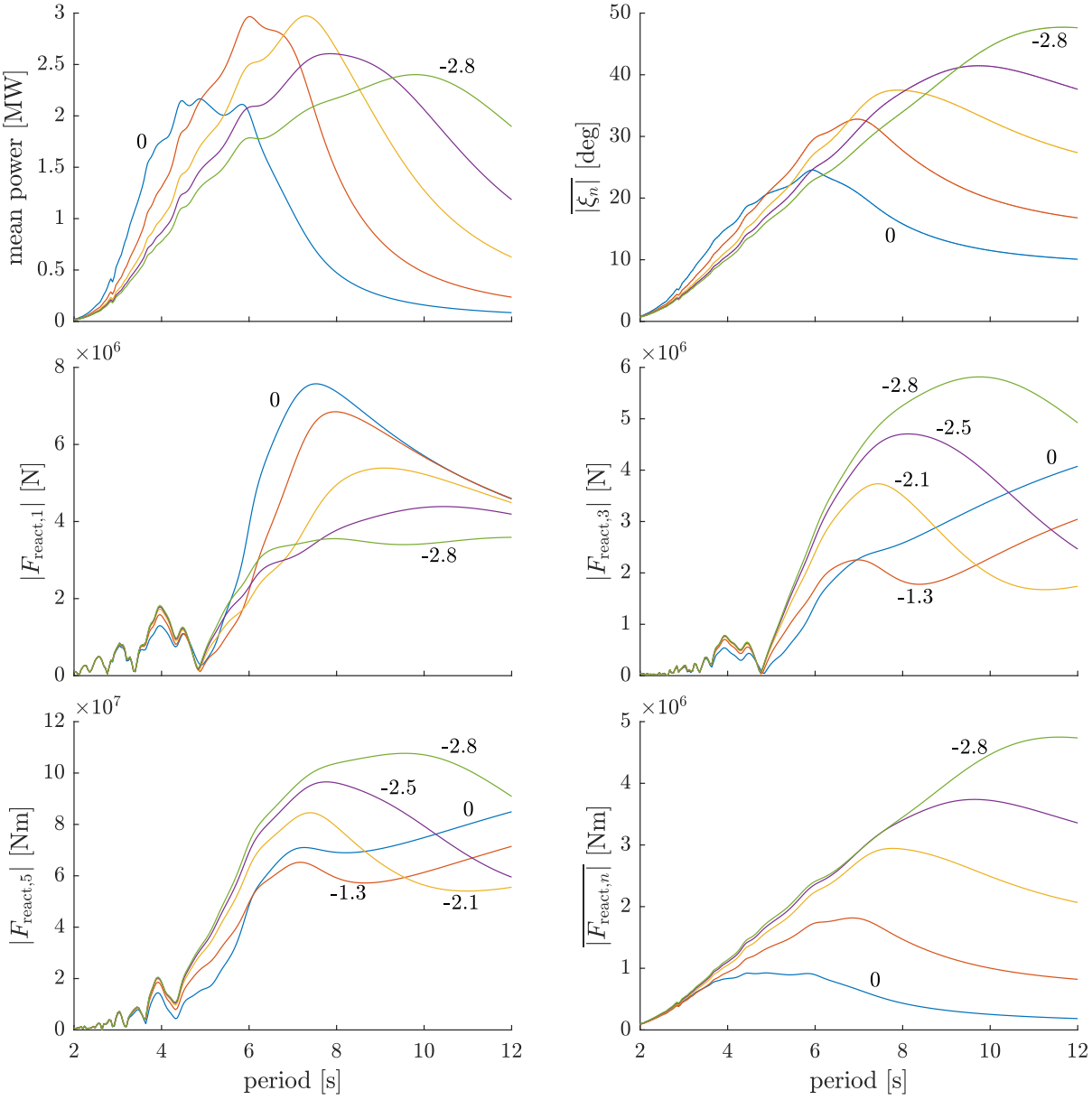

Figure 15. Mean absorbed power, duck displacement amplitudes, and reaction force (moment) amplitudes for a system identical to that in Fig. 14 but with the platform not allowed to move.

References

[1] X. Xiao, L. Xiao, and T. Peng. Comparative study on power capture performance of oscillating-body wave energy converters with three novel power take-off systems. *Renewable Energy*, 103:94–105, 2017.

[2] J. Falnes. *Ocean Waves and Oscillating Systems*. Cambridge University Press, Cambridge, UK, 2002.

[3] X. Zhang, J. Yang, and L. Xiao. Numerical study of an oscillating wave energy converter with nonlinear snap-through power-take-off systems in regular waves. *Journal of Ocean and Wind Energy*, 1(4):225–230, 2014.

[4] J. H. Todalshaug, G. S. Ásgeirsson, E. Hjálmarsson, J. Maillet, P. Möller, P. Pires, M. Guérinel, and M. Lopes. Tank testing of an inherently phase-controlled wave energy converter. *International Journal of Marine Energy*, 15:68–84, 2016.

[5] S. Peretta, P. Ruol, L. Martinelli, Amélie. Tetu, and J. P. Kofoed. Effect of a negative stiffness mechanism on the performance of the WEPTOS rotors. In *International Conference on Computational Methods in Marine Engineering*, pages 58–72. CNR, 2015.

[6] S. H. Salter. Wave power. *Nature*, 249:720–724, 1974.

[7] B. M. Count. On the dynamics of wave-power devices. *Proceedings of the Royal Society of London. Series A, Mathematical and Physical Sciences*, 363(1715):559–579, 1978.

[8] A. E. Mynett, D. D. Serman, and C. C. Mei. Characteristics of Salter's cam for extracting energy from ocean waves. *Applied Ocean Research*, 1(1):13–20, 1979.

[9] M. Katory and A. A. Lacey. Application of the two-dimensional Green's function to the hydrodynamic analysis of wave-energy devices. In K.-G. Jansson, J. K. Lunde, and T. Rindby, editors, *Proceedings of the First Symposium on Wave Energy Utilization*, pages 114–126, Gothenburg, 1979.

[10] S. H. Salter. Recent progress on ducks. *IEE Proceedings A-Physical Science, Measurement and Instrumentation, Management and Education-Reviews*, 127(5):308–319, 1980.

[11] D. D. Serman and C. C. Mei. Note on Salter's energy absorber in random waves. *Ocean Engineering*, 7(4): 477–490, 1980.

[12] M. J. L. Greenhow. Efficiency calculations for a Salter's duck on a compliant axis. *Applied Ocean Research*, 3(3):145–147, 1981.

[13] D. Skyner. Solo duck linear analysis. Technical report, University of Edinburgh wave energy project, 1987.

[14] D. Pizer. Numerical modelling of wave energy absorbers. Technical report, University of Edinburgh wave energy project, 1994.

[15] F. Ferri, A. Pecher, and J. P. Kofoed. Numerical analysis of a large floating wave energy converter with adjustable structural geometry. In *The 25th International Offshore and Polar Engineering Conference*. International Society of Offshore and Polar Engineers, 2015.

[16] J. Wu, Y. Yao, L. Zhou, N. Chen, H. Yu, W. Li, and M. Göteman. Performance analysis of solo Duck wave energy converter arrays under motion constraints. *Energy*, 139:155–169, 2017.

[17] R. Ramlan, M. J. Brennan, B. R. Mace, and I. Kovacic. Potential benefits of a non-linear stiffness in an energy harvesting device. *Nonlinear Dynamics*, 59(4):545–558, 2010.

[18] J. N. Newman. Wave effects on deformable bodies. *Applied Ocean Research*, 16:47–59, 1994.

[19] A. Pecher, J. P. Kofoed, and T. Larsen. Design specifications for the Hanstholm WEPTOS wave energy converter. *Energies*, 5(4):1001–1017, 2012.

[20] WAMIT. *User Manual*. WAMIT, Inc., Chestnut Hill, MA, 2016. URL `http://www.wamit.com`. Version 7.2.